A Model of the Foot and Ankle In Running

Bo Waggoner

Advisor: E. L. Bouzarth

April 25, 2011

Submitted for Graduation with Distinction
Department of Mathematics
Duke University
Durham, NC

1 Abstract

We present several variations on a model and simulation of the foot and ankle during the course of one running stride. We summarize the motivation behind the model and similar work in the field, then describe the model and the results obtained. In the model, the shin and foot are each represented by thin rods, while two major muscle groups are modeled as exponential springs. The ground is modeled as a network of points connected by damped linear springs. Results on ground impact forces and physiological parameters are presented. In particular, we find that heel striking tends to produce higher peak impact forces than forefoot striking, we search for foot parameters producing the most effective foot strike, we compare force-time data obtained to experimental results, and we compare the effects of different ground and shoe properties on foot strike.

2 Motivation

Running is one of humanity's simplest and most natural activities. In fact, some researchers believe that distance running ability was a central influence on human evolution [1]. However, there is much to learn about the mechanics of human running on the level of the foot and ankle. Although there is a body of research that models the entire leg as a spring [2], less is known about the process of foot striking. For example, there remain open basic questions such as: what differences are caused by either heel striking (in which the heel is the first part of the foot to hit the ground) or forefoot striking; what effects running shoes of various properties have, especially on those two footstrike patterns; the effect of various anatomical parameters, such as heel length, on landing and takeoff; and, if running was an influence on human evolution, what traits in the foot were selected for and why? Answers to these questions may be relevant in fields of evolutionary biology and anthropology, performance in sport, injury prevention and treatment in sport, and footwear and running surface design.

Much research in this area is experimental in nature, *e.g.* measuring the force of impact of a runner's foot on the ground with different footstrike patterns [3]. Some have investigated experimentally measuring internal forces in the leg in dancing [4]. In contrast to these experimental approaches, there is also research on modeling the foot, but generally in a walking context and

rarely in a running context [5, 6, 7, 8, 9]. We have found only two examples of models of the foot designed to ask questions about footstrike in running. One of these is a mathematical model which only considers initial ground impact and no subsequent properties of footstrike [1]. The other is a simulation, but focuses solely on heel striking [6].

A mathematical model and simulation may be able to shed light on these questions in ways that experiments cannot. For example, it could make a statement regarding internal forces between bones at the ankle or knee that are not easily measurable experimentally. To better understand the function of the human foot, such a model could also allow testing of nonphysical physiological parameters: by testing parameters not found in humans (*e.g.* very long toes or heels), we might better understand why the foot is shaped as it is. Similarly, a model would allow testing of shoe and surface properties which do not yet exist, without incurring the expense of actually producing these items. Finally, a model that closely mimics real-life phenomena may provide insight into the fundamental mechanism of running by, for example, shedding light on how and when different muscles fire at different points in a running stride.

Therefore, our goal is to present a model that addresses some of these questions and allows for future extension. We consider several variations of the model and how they might shed light on these issues, and comment on possible future work.

3 Models

We consider three different models. The first, which we call the Basic Model, is the simplest; the other two are extensions of the first. The Basic Model incorporates the foot and shin along with two muscle groups. The other two models extend this model in different ways. The second model, called the Body Model, extends the Basic Model by incorporating the thigh, muscles of the thigh, and the body. The third model, called the Shoe Model, extends the Basic Model by incorporating a shoe attached to the foot. All three models represent the ground as a network of points connected by linear springs. We describe each model in turn.

3.1 The Basic Model

3.1.1 The Lower Leg

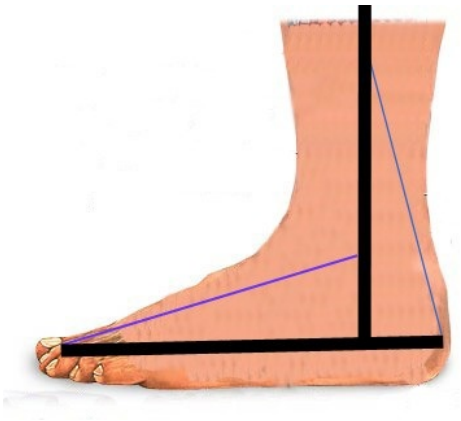

Figure 1: The lower leg, adapted from [10].

In the Basic Model, we model the shin, ankle, and foot. The basic correspondence of these components with the physical leg are show in Figure 1. The Body Model and Shoe Model incorporate additional structures. For all models, we simulate motion of the lower leg over the course of one foot strike. Figure 2 demonstrates a sample forefoot strike, in which the forefoot is the first part of the foot to make contact with the ground.

The Basic Model consists of two rods and two springs, as depicted in Figure 3. One rod repesents the the shin, and the other, the foot. The rod constituting the shin is referred to as the shank. It models both bones of the lower leg, the tibia and fibula. The rod modeling the foot is a simplification

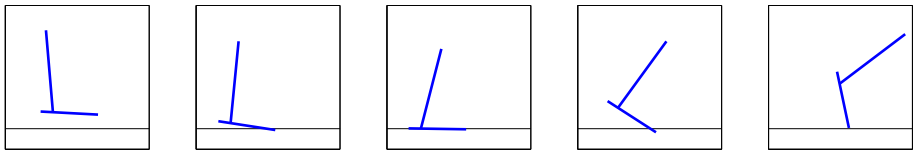

(a) Falling (b) Touchdown (c) Stance (d) Push Off (e) Float

Figure 2: Stages of the simulation demonstrating a forefoot strike, where the forefoot is the first part of the foot to touch the ground.

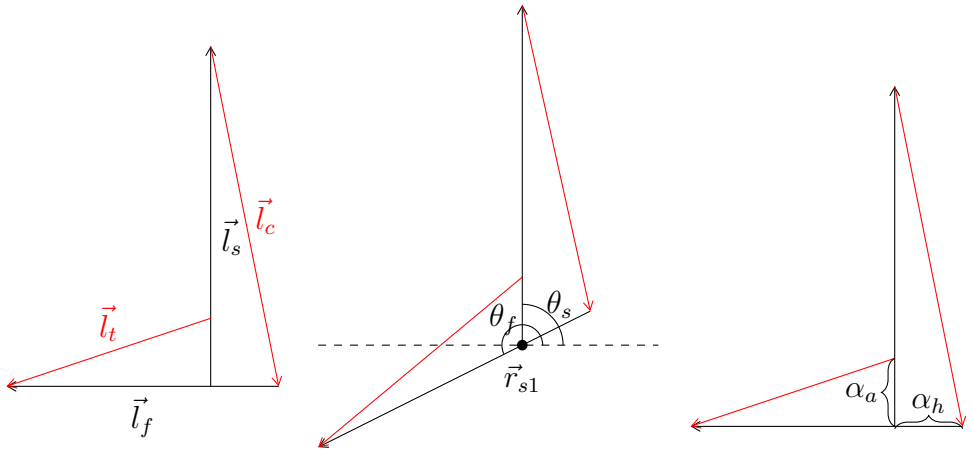

(a) Vectors of the model. (b) Variables of the model. (c) Ratios of the model.

Figure 3: The model is a simplification of the human lower leg. (a) Bones are modeled as $\vec{l}_s$, the shank, and $\vec{l}_f$, the foot. Muscles are $\vec{l}_c$, the calf group, and $\vec{l}_t$, the tibialis group. (b) θ_f is the angle of the foot and θ_s the angle of the shank with respect to the horizontal axis. $\vec{r}_{s1}$ is the position of the contact point between the foot and the shank. (c) α_a is the ratio of ankle height to total shank height, while α_h is the ratio of heel length to total foot length.

of the 26 bones and other structures of the foot[1]. Both the foot and the shank are treated as thin rods of constant density.

Each of the springs models a different muscle group. One spring represents the calf muscles, the soleus and the gastrocnemius. These muscles are responsible for the extension of the foot during movements such as pointing the toe and pushing off from the ground. The second spring represents the muscles responsible for dorsiflexion of the foot (pulling the toe forward and upward), such as the tibialis anterior, among others [11]. These muscles are modeled as exponential springs, based upon a model presented by McMahon

[1]While these complex structures may play significant roles in foot strike, the simplification may still be reasonable. Consider, for example, a foot shod in a typical running shoe: Insofar as contact with the ground, it resembles a flat rod more than a bare foot.

[2]. The force generated by the springs is given by:

$$\vec{F}_{spr} = \mu \left(e^{\alpha \frac{|\vec{l}|}{|\vec{l}_0|}} - e^{\alpha} \right) \hat{l} \quad , \tag{1}$$

where $\left|\vec{l}_0\right|$ is the resting length of the spring, $\left|\vec{l}\right|$ is the current length of the spring, $\hat{l}$ is the unit vector in the direction of the spring, and μ and α denote spring properties.

There are three types of external forces acting on the lower leg: gravity ($\vec{F}_{gravity}$), force of contact with the ground ($\vec{F}_G$), and external forces imposed at the top of the shank and ankle ($\vec{F}_{ext1}$ and $\vec{F}_{ext2}$). These external forces will enforce the condition that the shank rotates at a constant angular velocity throughout the simulation; this is our boundary condition modeling the motion of the body above the knee. Therefore, the angular velocity of the shank, ω_s, is a constant and its angular acceleration, α_s, is zero throughout the simulation. $\vec{F}_{ext1}$ and $\vec{F}_{ext2}$ contribute no net force, as they are constrained to sum to zero, but they do produce net torque.

Internal forces include the spring forces of the calf group ($\vec{F}_{calf}$) and tibialis group ($\vec{F}_{tib}$), as well as a force at the ankle ($\vec{F}_{ankle}$). This latter force models structures connecting the foot and the shank, and imposes the condition that the foot and shank must remain attached. By Newton's third law, the force exerted by the foot on the shank is equal and opposite to that by the shank on the foot; $\vec{F}_{ankle}$ is this force.

3.1.2 Equations of Motion and the Simulation

Given the physiological parameters of the model, the system's physical configuration at any time is a function of three variables: $\vec{r}_{s1}$, θ_s, and θ_f, depicted in Figure 3(b). $\vec{r}_{s1}$ denotes the coordinates of the point of contact between the shank and the foot; θ_s is the angle of the shank with respect to the x-axis; and θ_f is the angle of the foot with respect to the x-axis. In the Basic Model and Shoe Model, the shank rotates at a constant angular velocity ω_s, so θ_s is known at any particular time. Given these variables, we can calculate the position of all other points on the lower leg, such as the center of mass of one of the rods. Thus we say that these three variables give the lower leg's current configuration.

From the current configuration, we can calculate the muscle forces $\vec{F}_{calf}$ and $\vec{F}_{tib}$. We also can calculate the ground force $\vec{F}_G$ and torque $\vec{\tau}_G$, as

discussed in Section 3.1.3. The unknown forces are the force at the ankle, $\vec{F}_a$, and the external forces, $\vec{F}_{ext1}$ and $\vec{F}_{ext2}$.

The model gives us constraints on the configuration and the change in configuration over time. It includes Newton's second law (Equation (2)) and its rotational analogue (Equation (3)) for the shin and the shank. Thus for both the shank and the foot we will have equations of the form

$$\vec{F}_{net} = m\vec{a} \quad , \tag{2}$$

$$\vec{\tau}_{net} = \vec{I}\alpha \quad , \tag{3}$$

where $\vec{\tau}$ is torque, α is angular acceleration, and $\vec{I}$ is the moment of inertia tensor.

We use these equations to run the simulation. At a certain time k, we have the current configuration of the system: $\vec{r}_{s1}$, θ_f, and θ_s (which also determine some of the forces). Solving the system of equations in the model gives us the acceleration of the point $\vec{r}_{s1}$ and the angular acceleration of θ_f at time k. It also gives us the values of the unknown forces at time k. We give the system of equations in terms of the acceleration of the center of mass of the foot, $\vec{a}_f$, and of the shank, $\vec{a}_s$, but when solving the equations, these are expanded out as functions of the acceleration of the point $\vec{r}_{s1}$ and the angular acceleration of the foot α_f.

The complete system of equations is:

$$m\vec{a}_f = \vec{F}_{calf} + \vec{F}_{tib} + \vec{F}_{ankle} + \vec{F}_{gravity} + \vec{F}_G \quad , \tag{4}$$

$$m\vec{a}_s = -\vec{F}_{calf} - \vec{F}_{tib} - \vec{F}_{ankle} + \vec{F}_{gravity} \quad , \tag{5}$$

$$\vec{I}_f\alpha_f = \frac{-\vec{l}_f}{2} \times \vec{F}_{calf} + \frac{\vec{l}_f}{2} \times \vec{F}_{tib} + \left(\alpha_h - \frac{1}{2}\right)\vec{l}_f \times \vec{F}_{ankle} + \vec{\tau}_G \quad , \tag{6}$$

$$\begin{aligned} \vec{0} = {} & \frac{-\vec{l}_s}{2} \times \vec{F}_{calf} + \frac{\vec{l}_s}{2} \times \vec{F}_{ext1} + \left(\frac{1}{2} - \alpha_a\right)\vec{l}_s \times \vec{F}_{tib} \\ & + \left(\alpha_a - \frac{1}{2}\right)\vec{l}_s \times \vec{F}_{ext2} + \frac{\vec{l}_s}{2} \times \vec{F}_{ankle} \quad , \end{aligned} \tag{7}$$

$$\vec{0} = \vec{F}_{ext1} + \vec{F}_{ext2} \quad , \tag{8}$$

$$0 = \vec{l}_s \cdot \vec{F}_{ext1} \quad . \tag{9}$$

The physiological parameters in the equations include α_a and α_h, which are the ratios, respectively, of ankle height to shank height, and heel length

to foot length, as shown in Figure 3(c). The variables $\vec{r}_f$ and $\vec{r}_s$ are the locations of the centers of mass of the foot and shank, respectively. θ_f is the current angle of the foot with respect to the horizontal axis. Also included implicitly are the physiological parameters of the lengths of the foot and shank, $\left|\vec{l}_f\right|$ and $\left|\vec{l}_s\right|$ respectively. The vectors $\vec{l}_f$ and $\vec{l}_s$ in the above equations are calculated from these lengths along with θ_f, and θ_s.

Equations (4) and (5) are applications of Newton's second law of motion, $\vec{F} = m\vec{a}$, to the foot and the shank respectively. Equations (6) and (7) are the rotational analogues of (4) and (5), stating that net torque on each rod is equal to the moment of inertia of the rod times the angular acceleration of that rod about its center of mass. In Equation (7), the net torque is zero because we have imposed a constant angular velocity on the shank, so that it rotates at constant speed.

Equation (8) enforces the constraint that the external forces contribute no net force. Equation (9) additionally enforces that the external forces must be perpendicular to the shank.

Having calculated the acceleration of our coordinates at time k, we use a finite difference method with time-step h to calculate the values of the coordinates at the next time-step:

$$\vec{x}_{k+1} = h^2\vec{a}_k + 2\vec{x}_k - \vec{x}_{k-1} \quad , \tag{10}$$

$$\theta_{k+1} = h^2\alpha_k + 2\theta_k - \theta_{k-1} \quad . \tag{11}$$

In this way, we obtain the configuration of the system at time $k+1$, advancing our simulation.

3.1.3 Modeling The Ground

In the Basic Model, the ground is modeled as a network of interconnected points, as shown in Figure 4. We may choose how dense this network is both horizontally and vertically by adding additional points and springs. In Figure 4, the ground is divided into ten columns and two rows of points. However, we have considered as many as 120 columns and five rows. In all cases, the line of points at the very bottom, far right, and far left are fixed in place; these are our boundary conditions on the ground.

Each spring is connected with linear springs to five neighbors, if it is in an outer edge (top, bottom, left, or right), or eight neighbors, if it is in a middle row. In the absence of any interaction with the foot, these points,

given very small masses, are free to move under the influence of these springs and gravity. Additionally, we introduce a drag force to these points. Thus, by summing over all neighboring springs s, the net force on the ith point is given by:

$$\vec{F}_{net} = \sum_s \vec{F}_{si} - b\,\frac{d\vec{r}_i}{dt} \quad , \tag{12}$$

$$\text{where} \quad \vec{F}_{si} = -k\left(\left|\vec{l}\,\right| - \left|\vec{l}_0\right|\right) \quad . \tag{13}$$

b is the drag coefficient, k is the spring constant, $\left|\vec{l}_0\right|$ is the length of the spring at rest, $\left|\vec{l}\,\right|$ is the current length of the spring, and $\frac{d\vec{r}_i}{dt}$ is the velocity of the ith point.

When the foot comes into contact with the ground, their interaction is modeled in the following way. When some part of the rod modeling the foot passes below one of the ground's points, that point becomes "stuck" to the foot. When the foot lifts off above that point's resting position, moving upwards, that point becomes unstuck.

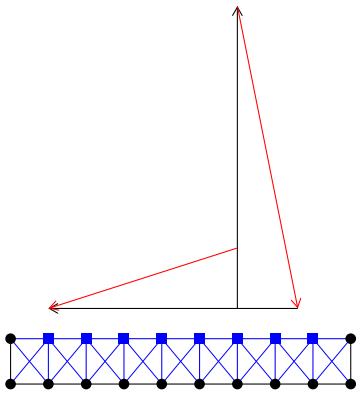

Figure 4: Modeling the ground. The points shown as black circles at the far bottom, left, and right are fixed, while the blue squares may move.

With this model, the force of the ground on the foot, $\vec{F}_G$, is equal to the sum over all stuck points of the net force on those points. Each of these forces is given by Equation (12). Similarly, the torque of the ground on the foot, $\vec{\tau}_G$, is equal to the sum of the torques of the stuck points. The torque

of a point is given by:

$$\vec{\tau} \;=\; \vec{r_p} \times \vec{F_p} \quad , \tag{14}$$

where $\vec{r_p}$ is a vector from the foot's center of mass to the point, and $\vec{F_p}$ is the force on that point.

Throughout the time that a point is stuck to the foot, we treat it as having zero mass; it does not change the motion of the foot and does not have any motion of its own. All unstuck points have a very small mass which is used in determining their motion by Newton's Second Law.

3.2 The Body Model

This model treats the upper leg and body in more detail than the first. In the Basic Model, we used external forces to model the effects of the upper leg and body. These forces enforced the constraint that the shank (shin) rotates at a constant angular velocity. Now that we model the femur and body explicitly, we drop the external forces $\vec{F}_{ext1}$ and $\vec{F}_{ext2}$. There is no additional constraint on the rotation of the shank, as there was in the Basic Model. The only external forces acting on the Body Model are that of gravity and the ground.

We represent the thigh as a thin rod of constant density, representing the femur and other structures of the upper leg, as shown in Figure 5. The body is modeled as a point mass attached to the end of the upper leg. Muscles of the upper leg responsible for interaction between the lower and upper leg, such as the hamstring and quadriceps groups, are modeled as a single linear spring connecting the upper and lower leg.

This model has an additional degree of freedom, described by the variable θ_b. This denotes the angle of the femur with respect to the horizontal. Thus, we say that the configuration of the Body Model is given by $\vec{r}_{s1}$, θ_f, θ_s, and θ_b. We also have additional parameters (constants) to describe the two attachment points of the upper leg muscle: α_{qs} for the location on the shank, and α_{qb} for the location on the femur. We also have parameters describing the spring constants of this muscle, which produces a force $\vec{F}_{quad}$. This muscle group is modeled as a linear spring. There is also a force of contact $\vec{F}_k$ at the knee, between the shank and the femur, which enforces the constraint that the two bones are connected at the knee.

The equations governing the Body Model are similar in form to those of the Basic Model. In the body case, however, we have three net force and

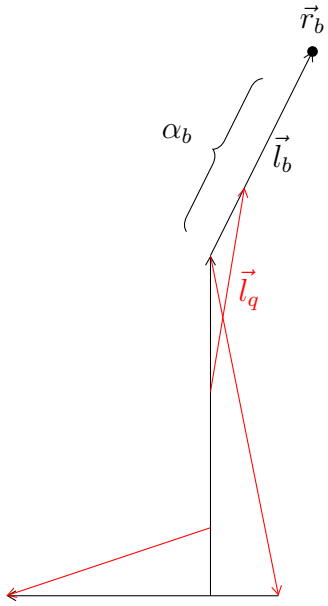

Figure 5: The Body Model. $\vec{l}_b$ denotes the thigh, $\vec{l}_q$ denotes the upper leg muscles, and $\vec{r}_b$ denotes the location of the body mass. α_b describes the location of the center of mass of the femur-body system.

three net torque statements: one of each for the foot, the shank, and the femur-body system. These are given by Equations (15) - (20). The ground and its interactions with the foot are modeled in the exact same way as in the Basic Model.

$$m\vec{a}_f = \vec{F}_{calf} + \vec{F}_{tib} + \vec{F}_{ankle} + \vec{F}_{gravity} + \vec{F}_G \quad , \tag{15}$$

$$m\vec{a}_s = -\vec{F}_{calf} - \vec{F}_{tib} - \vec{F}_{ankle} + \vec{F}_{gravity} - \vec{F}_{knee} - \vec{F}_{quad} \quad , \tag{16}$$

$$m\vec{a}_{qb} = \vec{F}_{gravity} + \vec{F}_{knee} + \vec{F}_{quad} \quad , \tag{17}$$

$$\vec{I}_f\alpha_f = \frac{-\vec{l}_f}{2} \times \vec{F}_{calf} + \frac{\vec{l}_f}{2} \times \vec{F}_{tib} + \left(\alpha_h - \frac{1}{2}\right)\vec{l}_f \times \vec{F}_{ankle} + \vec{T}_G \quad , \tag{18}$$

$$\begin{aligned} \vec{I}_s\alpha_s = {} & \frac{-\vec{l}_s}{2} \times \vec{F}_{calf} + \left(\frac{1}{2} - \alpha_a\right)\vec{l}_s \times \vec{F}_{tib} \\ & + \frac{-\vec{l}_s}{2} \times \vec{F}_{knee} + \left(\frac{1}{2} - \alpha_{qs}\right)\vec{l}_s \times \vec{F}_{quad} + \frac{\vec{l}_s}{2} \times \vec{F}_{ankle} \quad , \end{aligned} \tag{19}$$

$$\vec{I}_{qb}\alpha_{qb} = (-\alpha_b)\,\vec{l}_b \times \vec{F}_{knee} + (\alpha_{qb} - \alpha_b)\,\vec{l}_b \times \vec{F}_{quad} \quad . \tag{20}$$

$\vec{r}_{bf}$ is the location of the center of mass of the femur-body component, while α_b describes where along the femur this center of mass is located. Each component of the system (the foot, the shank, and the femur-body) has two equations: a net-force equation in two dimensions, and a net torque equation in one dimension. These form a linear system of nine equations total. Equations (15) - (17) are vector equations in two dimensions. Equations (18) - (20) are three-dimensional, as they involve cross-products and torque, but they are non-trivial only in the z direction. These equations can be solved for the nine unknowns: $\vec{r}_{s1}$, θ_f, θ_s, θ_b (the variables describing the system's configuration), $\vec{F}_a$, and $\vec{F}_k$.

With this model, our simulation proceeds in the same fundamental way as in the Basic Model: Given the system's current configuration, we solve our system of equations to find the acceleration of $\vec{r}_{s1}$ and angular acceleration of θ_f, θ_s, and θ_b; then, we use a finite-difference method to obtain the configuration at the next time-step.

3.3 The Shoe Model

In this model, the motion of the lower leg is governed by the same equations as the Basic Model, Equations (4) - (9). The difference lies in the treatment

of the ground and force on the foot.

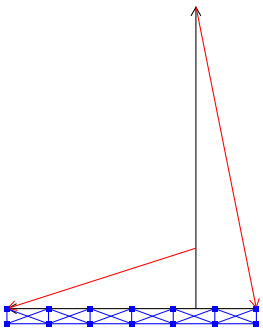

Figure 6: The Shoe Model.

As shown in Figure 6, the shoe is modeled in the same way as the ground – as a network of interconnected points. These points have a damping coefficient, and are connected to their neighbors via linear springs whose spring constants are predetermined. The top row of points remain permanently stuck to the foot, and are massless; they move with the foot. The force $\vec{F}_G$ exerted on the foot by the ground and shoe is determined by the total spring force on each point stuck to the foot. The torque $\vec{\tau}_G$ on the foot is determined by these forces along with the location of these points.

The points making up the shoe that are not stuck to the foot have a very small mass, and move according to the net force on them. This net force has three components: gravity, the total spring force, and the damping force. The total spring force is the sum of the forces of all springs to which that point is connected. The damping force is calculated from the average velocity of that point relative to its neighbors. (Thus, if every point on the shoe is moving with the same velocity, there is no damping force on any of the points.)

The interaction of the shoe with the ground is modeled in the following way. If a point in the shoe enters the ground area, it becomes connected to the nearest four points of the ground by linear springs of a predetermined spring constant. The springs' resting lengths are set equal to their lengths at this moment. The springs exert force on both the points of the shoe and those of the ground to which they are connected. At the time when the springs cease exerting an upward force on the shoe, they are removed and the shoe is allowed to "lift off" unrestrained.

4 Results

We consider several different questions about each model. With the Basic Model, we begin by describing reasonable parameters, which produce realistic behavior and force-time plots for a forefoot strike. We also consider the differences between a heelstriking and forefoot striking in terms of forces produced.

We then consider the parameters of an "optimal" lower leg. We evaluate a lower leg with a given set of parameters on the basis of how far it bounces after pushing off from the ground. We use several methods to determine the most optimal set of parameters we can find for both a forefoot strike and a heel strike using the Basic Model.

With the Body Model, we determine how modeling the femur and body causes changes from the results obtained with the Basic Model. We specifically consider the behavior of the ground, ankle, and knee forces over time. We also consider how the behavior of the Body Model is affected by varying ground properties.

With the Shoe Model, treating the shoe as a network of points connected to the foot, we compare force plots obtained to those of the Basic Model. We then consider the effect of shoes of different shapes, but identical properties, on footstrike.

All distances given are measured in meters, forces are in Newtons, and time is in seconds.

4.1 The Basic Model

4.1.1 Introduction

With the Basic Model, we examine several different fundamental questions. In particular, we begin by considering the impact of a footstrike by plotting the force of the foot on the ground over time.

The amount of force between the ground and the foot over the course of one stride is an important result and has been documented in the literature[1]. Figure 7 gives an example from The Harvard Skeletal Biology Lab of experimental data showing this force over the course of two foot strikes[1]. This particular plot is from a heel strike: the heel was the first part of the foot to hit the ground. The impact of the heel caused an initial spike in the amount of force, which the researchers call an "impact transient". They found no

impact transient during forefoot strikes; the force plot consisted of a single smooth peak. The first question we ask of our model, therefore, is how well it replicates these types of results.

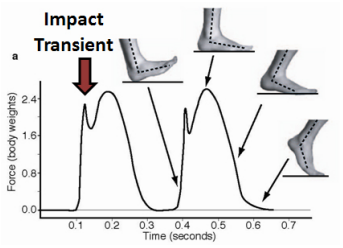

Figure 7: An experimental plot of force versus time [1].

However, we also examine topics which have been addressed less often in experimental research. These include the behavior of forces at the ankle, which are difficult to measure experimentally. They also include the parameters of a foot which produce the "optimal" footstrike, all other conditions being equal.

4.1.2 Ground and Ankle Forces

With the Basic Model, we found it was possible to produce smooth force-time plots such as those found experimentally. However, the types of footstrikes in which this occurred were somewhat unrealistic; they tended to have less flexion of the foot at the ankle, so that, upon landing, the forefoot would contact the ground and bounce while the heel remained off of the ground.

Instead, we chose model parameters in order to produce more realistic motion (parameters displayed in Table 4). With these parameters, we found results such as those displayed in Figure 8. For both the forefoot and heel strike, the model tended to produce two peaks of force rather than one smooth peak. As we will show with the Body Model, more detailed modeling of the body may reduce this phenomenon, by incorporating the dynamics of absorbing the impact from the entire body rather than just the lower leg.

In addition to measuring ground impact force, we also examine the force at the ankle, $\vec{F}_{ankle}$. This force, connecting the foot and shank, may be considered a measure of how much internal stress the lower leg undergoes as a function of time. These plots are also included in Figure 8.

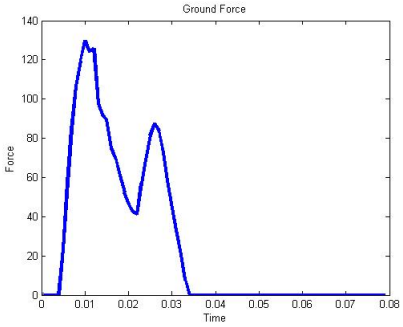

(a) Ground Force - Forefoot Strike

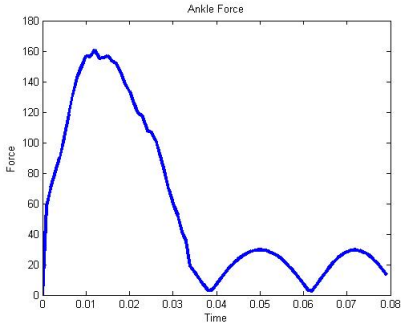

(b) Ankle Force - Forefoot Strike

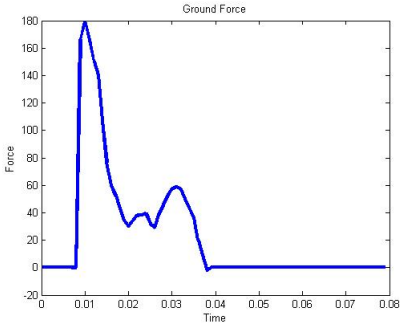

(c) Ground Force - Heel Strike

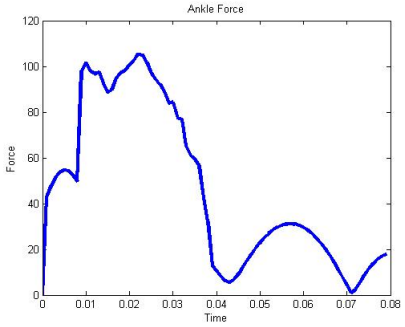

(d) Ankle Force - Heel Strike

Figure 8: Results of a typical simulation using the Basic Model. Force (N) versus time (s) is displayed for one simulated stride. Parameters for this simulation are given in Table 4. We use a time-step of 0.0001 seconds, and sample data for the plots at steps of 0.001 seconds.

4.1.3 Specific Differences Between Forefoot and Heel Strike

We found several consistent differences between forefoot strike and heel strike when using the same physical parameters. The force plots provided in Figure 8 demonstrate some of these differences. The ground impact force is significantly different for the two types of stride. In forefoot striking, the two force peaks tend to be closer together, and the minimum between these peaks tends to be higher. Overall, the force of the ground on the foot is smoother in the case of forefoot striking. Additionally, the peak impact force is lower in the case of forefoot striking. In Figure 8, the ground exerts a maximum force of approximately 130 Newtons on the forefoot striking model but approximately 180 Newtons on the heel striking model. However, the total impulse (amount of force times time) from the ground to the foot is similar in both cases, with the forefoot strike's amount being slightly higher.

The ankle force plot is similar in shape for both the forefoot and the heel strike cases. However, the ankle force at peak and total impulse is significantly less in the case of the heel strike. The peak is approximately 160 Newtons in the forefoot striking model but approximately 105 Newtons in the heel striking model. It may be of note that, in the heel striking case, the plot of force at the ankle versus time is much less smooth over time than the force in the forefoot-striking case.

4.1.4 Discussion of Differences

Some general conclusions can be clearly drawn from these results. In terms of ankle forces, a lower leg with the same physiological parameters tends to experience more force when forefoot striking than when heel striking. In terms of ground impact forces, the peak impact force is much higher in the case of heel striking.

However, the implications of these results on injury prevention are not necessarily clear. First, in our results for finding optimal parameters (discussed in Section 4.1.5), we find that ankle forces tend to be somewhat higher in the heelstriking case, rather than the forefoot-striking case. However, we again find that impact forces tend to be higher when heelstriking. Because of these results, we lend more importance to the difference in impact forces.

Additionally, we are uncertain which type of force is more injurous. Overuse injuries at the ankle are rare in runners; that is, ankle injuries tend to be caused by sudden impacts, and not by the long-term effects of many

miles of running. However, overuse injuries of the foot, such as metatarsal stress fractures, are relatively common. Higher ankle forces are therefore less of a concern than high impact forces. On the other hand, higher ankle forces may also mean that more force is propogated from the foot to the rest of the body. This may suggest a higher risk of injuries such as shin splints, stress fractures in the shin, and knee injuries from overuse.

Overall, we suggest that higher peak ground impact forces are more likely to be injurous to runners. For two runners of the same mass to run the same distance, they must impart about the same total impulse to the ground and receive the same total impulse back to keep aloft and moving forward. If one becomes injured and the other does not, the reason may be that the first experiences a higher peak force of impact. According to our results, this occurs more often with a heel strike, all other conditions being equal. For this reason, we conclude that heel strike may have a higher potential for producing overuse injuries than forefoot strike.We discuss potential complications to these results in Section 5.

4.1.5 Finding Optimal Parameters

With a given ground configuration and initial type of landing (heel or forefoot strike), we are interested in finding the optimal physical parameters of the model. Here, we define optimal as bouncing the farthest forward after a foot strike. We considered varying the following parameters: α_h, the ratio of heel length to foot length; α_a, the ratio of ankle height to shank height; θ_{f0}, the initial angle of the foot; and the elastic properties of both muscles (l_0, μ, and α in Equation (1)).

To attempt to find an optimal set of parameters with the criterion of furthest distance bouncing, we used two different algorithms: genetic and gradient optimization. In both cases, we set reasonable limits on the parameters in order to eliminate completely nonphysical solutions such a very large inital angle of the foot or an extremely large peak impact force. However, in both cases the algorithm produced relatively moderate values for optimal spring constants and ratios.

4.1.6 The Genetic Algorithm

Genetic algorithms search a large space of parameters by creating initial random sets of parameters and testing their fitness according to some prede-

Parameter	Forefoot Strike	Heel Strike	Description
α_h	0.1276	0.2389	ratio of heel length to foot length
α_c	4.0000	3.4017	spring property of calf group
μ_c	-4.3358	-4.8196	spring property of calf group
α_a	0.0286	0.0227	ratio of ankle length to shank length
α_t	0.1312	1.5884	spring property of tibialis group
μ_t	-3.5031	-0.0106	spring property of tibialis group
θ_{rest}	1.1832π	1.1987π	resting angle between foot and shank
θ_{f0}	1.0032π	0.9732π	initial angle between foot and shank
distance	0.2601	0.1444	distance forward the lower leg bounced

Table 1: Optimal parameters found by the genetic algorithm in the case of forefoot striking and heel striking. Also given is the distance forward bounced by each lower leg with those parameters.

fined metric. The sets of parameters that acheive the highest fitness scores are combined and perturbed to produce another group. Each member of this group is tested for fitness, and the process is repeated, producing improved groups at each step [12]. In this case, twenty different lower legs were produced with random initial parameters distributed normally around a typical set of parameters. Each of these twenty cases was simulated and the distance traveled after bounce was measured. Those traveling farthest were recombined, along with some random perturbation, to produce another twenty models, and so on.

One advantage of this approach is that it examines many different areas of the search space. Our search space consisted of all possible values of each of the parameters mentioned above. A genetic algorithm is less likely to become trapped at a local optimum, because it continually perturbs and recombines parameters. However, there is no guarantee that the parameters found after many generations is actually optimal in either a global or local sense. The final set of parameters is not necessarily the best possible. However, the parameters do improve at each step of the algorithm.

We used this algorithm to search for an optimal heel striking model and forefoot striking model. The parameters found are given in Table 1 and the results of a simulation with these parameters are given in Figures 9 and (10).

Both the heel strike and forefoot strike searches found models with very low ankles, as compared to the actual value for humans. However, it was also observed that varying ankle height, as well as the strength of the tibialis

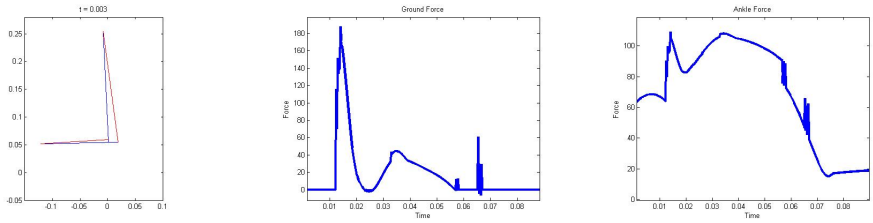

(a) Model (b) Ground Force (c) Ankle Force

Figure 9: Results for the genetic algorithm's optimal set of parameters with a forefoot strike.

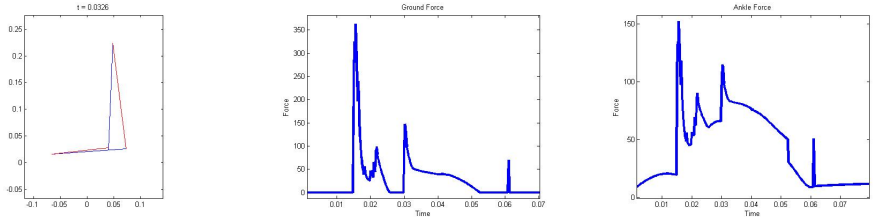

(a) Model (b) Ground Force (c) Ankle Force

Figure 10: Results for the genetic algorithm's optimal set of parameters with a heel strike.

muscle group, had only a small effect on the distance bounced. So it is likely that this result is unimportant in determining optimal foot parameters, especially from an evolutionary point of view.

Both models also found relatively small ratios of heel length to foot length (α_h). However, this ratio was quite different between foot strike patterns, as shown in Table 1. The forefoot strike selected for a significantly shorter heel than the heel strike. The actual physical value is likely to be somewhere between these two values, but we have not found published results for this ratio.

Interestingly, both foot strike types found approximately the same value for the resting position of the two springs, which occured when the foot was at an angle of approximately 0.7π radians (125°) to the shank. They found different results for the other spring constants of the calf muscles, but this is not surprising; these muscles attach at the heel, and so the different heel lengths of the two models will be related to the different spring constants.

For these two sets of parameters, the heel strike set and the forefoot strike set, we considered the ground impact force and internal ankle force over time. Once again, as shown in Figures 9 and 10, the heel strike produces significantly higher peak impact forces: approximately 360 Newtons compared to approximately 190 N for the forefoot strike. This time, however, the heel strike model produces somewhat higher internal ankle forces: approximately 150 Newtons versus approximately 110 N for the forefoot strike. Most notably, the forefoot striking model bounces farther: 0.260 meters versus 0.144 meters. This suggests that the forefoot strike is more efficient in terms of horizontal distance covered per stride, as both lower leg simulations began at the same height. We cannot definitively state this conclusion, as the heel striking and forefoot striking lower legs had different initial angles of the shank and foot, which may have affected the distance bounced. However, the large difference between the two results certainly lends strong credence to the hypothesis that forefoot striking is more efficient. In the future, this hypothesis could be tested by comparing the kinetic and potential energies of both models in addition to stride distance.

4.1.7 The Gradient Optimization Algorithm

The second method we used to find optimal parameters is more rigorous, but also more limited. We simply began with an initial, typical set of parameters, and slowly improved it using a finite-difference method. To do so,

we determined the gradient of the distance bounced with respect to each parameter. By moving each parameter a small distance along the gradient, we achieved a better set of parameters (one which produced a longer stride). We then repeated the process until the gradient was zero; a small change in every parameter resulted in a smaller stride. The main disadvantage of this approach is that, while it is guaranteed to find an optimal solution, it may be only a locally optimal solution, not a globaly optimal one. The gradient optimization algorithm found parameters that were similar to those of the genetic algorithm in some respects, such as the plots of ground and ankle force. However, rather than comparing the results of this algorithm to those of the previous one, we will focus on comparing the heel striking and forefoot striking cases of this algorithm's results.

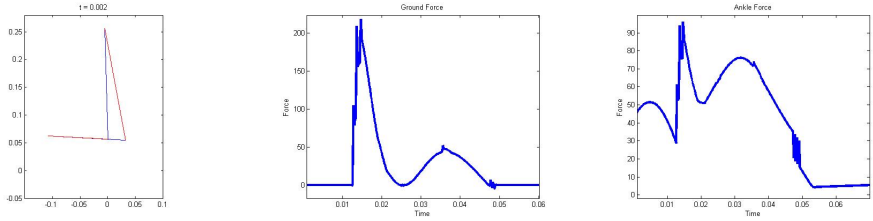

(a) Model (b) Ground Force (c) Ankle Force

Figure 11: Results for the gradient optimization algorithm's optimal set of parameters with a forefoot strike.

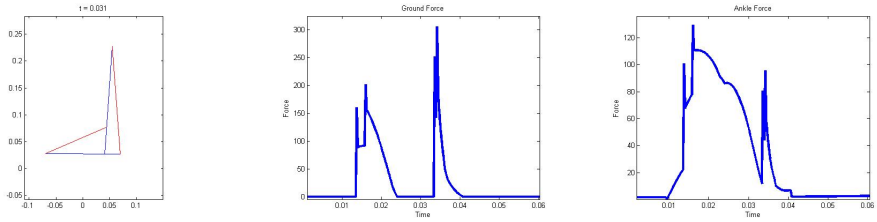

(a) Model (b) Ground Force (c) Ankle Force

Figure 12: Results for the gradient optimization algorithm's optimal set of parameters with a heel strike.

Figures 11 and 12 show the models and force-time plots produced by the parameters found. For the forefoot strike, the plot of ground forces versus time show a strong initial impact followed by a gradual takeoff. The heel

Parameter	Forefoot Strike	Heel Strike	Description
α_h	0.2270	0.2096	ratio of heel length to foot length
α_c	4.0358	4.5971	spring property of calf group
μ_c	-4.0128	-4.5964	spring property of calf group
α_a	0.0050	0.2500	ratio of ankle length to shank length
α_t	2.9674	3.0000	spring property of tibialis group
μ_t	-1.9895	-1.9958	spring property of tibialis group
θ_{rest}	1.0506π	0.9549π	resting angle between foot and shank
θ_{f0}	0.9792π	1.0506π	initial angle between foot and shank
distance	0.3684	0.0806	distance forward the lower leg bounced

Table 2: Optimal parameters found by the gradient optimization algorithm in the case of forefoot striking and heel striking. Also given is the distance forward bounced by each lower leg with those parameters.

strike shows a sudden impact of a similar magnitude, but a much larger, quicker force during takeoff. As in the case of the parameters found by the genetic algorithm, the plot for the forefoot strike is smoother. The ankle force plots are also similar to those of the genetic algorithm's parameters. The forefoot strike's plot is smoother, while that of the heel strike has multiple sharp peaks.

It should be noted that the gradient optimization algorithm found many different parameters from the genetic algorithm; these parameters appear in Table 2. In the case of heel striking, the gradient optimization algorithm found a significantly different result from the genetic algorithm, especially in ankle size. Its solution also produced a smaller distance bounced than that of the genetic algorithm. Because of this,we speculate that this solution may be optimal locally, but not globally.

The forefoot-striking parameters produced by the gradient optimization algorithm were similar to those of the genetic algorithm in appearance, but were different in certain significant ways. The gradient optimization algorithm's set of parameters included a somewhat larger heel. However, it had a smaller resting angle and a somewhat less stiff calf spring. These characteristics offset the larger heel to some extent in terms of torque produced by the calf muscle, so that the solutions of both models are likely quite similar in amount of torque produced at a given angle. However, the solution produced by the gradient optimization algorithm bounced much farther.

As in the results of the genetic algorithm, with the gradient optimization

algorithm we found the heel striking model to produce higher peak forces. From the ground, the heel striking lower leg underwent a peak force of approximately 300 Newtons, compared to approximately 215 Newtons for the forefoot striking lower leg. At the ankle, the heel striking lower leg underwent a peak force of approximately 125 Newtons, versus approximately 95 Newtons for the forefoot striking lower leg.

4.2 The Body Model

The Body Model makes a significant change to the Basic Model. By modeling the femur and body as physical elements attaching to the lower leg, rather than as a boundary condition imposed on the motion of the shank, we can obtain more realistic behavior in terms of force of impact. Additionally, we can better examine forces produced at the knee and by upper leg muscles, as well as the effect of different upper leg/body parameters on footstrike.

4.2.1 Forces in Footstrike

With certain parameters, the Body Model produces a force-time plot for ground forces that is very similar to those observed experimentally. Results for a typical simulation using these parameters are shown in Figure 13. We observe a quite small initial spike of force as the foot makes contact with the ground; however, after that, the force plot exhibits one peak. In this regard, the Body Model is significantly closer to experimental results than the Basic Model.

The ankle force plot in the case of the Body Model (Figure 13) is very similar to that of the Basic Model (as was shown in Figure 8). It shows a smooth peak of force during impact, followed by small oscillations after takeoff.

The plot of force at the knee over time exhibits oscillatory behaviour throughout the footstrike. Interestingly, a common pattern was one of alternating large and small oscillations of force at the knee.

Comparing magnitude of forces shows that the ankle experiences significantly more maximum force than the knee or foot. The maximum force on the foot during the typical simulation was about 662 Newtons. This peak occurred at time $t = 0.0201$ seconds. However, the maximum force on the ankle during this simulation was about 2751 Newtons. This occurred slightly later, at $t = 0.0247$ seconds, but at a time when foot force was still near its

k \ b	40	60	80	100
30,000	25.77	25.73	25.99	25.97
50,000	26.50	26.48	26.46	26.46
80,000	26.76	26.76	26.74	26.73

Table 3: Impulse of the ground on the foot for various values of the ground properties spring constant (k) and damping coefficient (b). Values are in Newton-seconds.

peak. The maximum force at the knee, meanwhile, was about 1048 Newtons. This occurred at $t = 0.0405$ seconds, while the foot was lifting off from the ground and impact forces were dropping. However, there was a smaller peak of knee force of about 952 Newtons at $t = 0.0198$ seconds, as ground impact force was reaching its peak.

These results suggest that knee, ankle, and foot forces are not necessarily well-correlated in time. They also suggest that internal forces at the knee and especially the ankle may be significantly higher than impact forces measured at the ground.

4.2.2 Varying Ground Properties

With the Body Model, we examined the effect of different ground properties on footstrike. Recall that the ground is represented by an array of points, each of which has a small mass and is connected by linear springs to its surrounding points. The strength of these springs is given by a spring constant k. Each point is also subject to damping forces inversely proportional to its velocity. The strength of the damping force is given by a damping constant b. The net force is given by Equation (12).

To determine how changes in these properties affected footstrike, we varied the spring constant and damping coefficient of the ground points while keeping all other parameters constant. We recorded the total impulse transmitted to the foot by the ground during the simulation. Impulse measures the total force over time, so the recorded value is $\int \left|\vec{F}_G\right| dt$, integrated from the time the foot first contacts the ground until it lifts off. The results are summarized in Table 3.

Impulse is measured in Newton-seconds, and it can also be interpreted as a total change in momentum. Thus the values given in Table 3 are the change in momentum of the foot due to its collision with the ground.

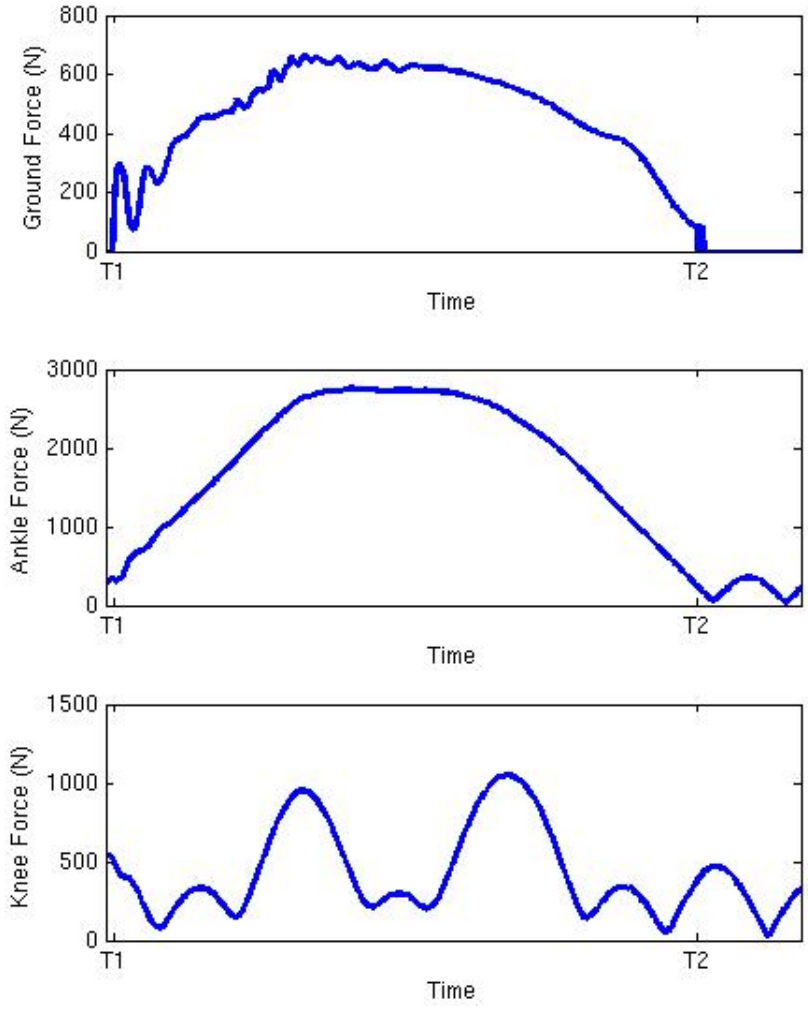

Figure 13: Results for a typical set of parameters using the Body Model (forefoot strike). Parameters for this model are given in Table 5. We use a time-step of 0.0001 seconds. Time $T1$ denotes touchdown of the foot, and time $T2$ denotes takeoff.

It is clear that total impulse increases with increasing spring constant. However, impulse does not vary significantly with a changing damping coefficient. This may suggest that high damping coefficients tend to cause a quick decrease in velocity upon landing, but have little effect on total impulse after that. During much of a footstrike, the foot actually moves very little, remaining almost "anchored" to the ground. The spring forces acting on the foot are generally transfered to the shank, femur, and body, resulting in changes in velocity for those elements. For the foot, after an initial deceleration phase, velocities are generally small. The size of the damping coefficient is no longer very important.

It is not immediately obvious why, for a given damping coefficient, higher spring constants impart higher impulses. In the absence of damping, one would expect all spring constants to impart the same total impulse, but to take different amounts of time to do so (normal harmonic oscillation). Each of the simulations above, however, takes approximately the same amount of time – the duration does not appear to depend on either the spring constant or the damping coefficient.

So why do higher spring constants produce higher total impulses? These results suggests that the damping force plays a more important role than spring force during landing and deceleration. The damping force may influence the duration and distance traveled during deceleration. Thus, ground simulations of different spring constants, but equal damping coefficients, would tend to compress the springs a similar distance during the initial deceleration phase. Then, once velocity is small, spring forces become more important. Springs with a higher spring force will impart more total force to the foot.

It is less clear how these results should be related to actual running and running surfaces. For instance, lower impulse means less force of impact over time. Thus, a lower impulse may appear to be beneficial from an injury standpoint. But lower impulse also means a smaller change in momentum. This would mean that a runner, using the same footstrike pattern, loses more energy to damping and gets less "bounce" or return from the ground.

Meanwhile, it is not immediately clear how our properties of spring constants and damping coefficients relate to actual ground properties. More work will need to be done in this area to identify actual surfaces corresponding to our results.

4.3 The Shoe Model

The Shoe Model made changes to the Basic Model which seemed simple, but produced a variety of results. When modeling the shoe as a lattice of points, in a similar way to the ground, the simulation behaved quite differently. We first present some results for a simulation of a forefoot strike using typical parameters for the Shoe Model and then compare these results for differently shaped shoes. This investigation is motivated by running shoe designs, which vary in thickness at the heel and at the forefoot.

4.3.1 Forces in Footstrike

We found that the Shoe Model was significantly less able to emulate experimental ground-force plots than the Basic Model and Body Model. Plots of the ground impact and ankle forces are given in Figure 14. The ground force is measured as the force between the points of the shoe and the ground. It has two main peaks of force, but also has many rather jagged peaks as well. This result is caused by the very elastic nature of the shoe model. For a large variety of parameters, we found that simulations of the shoe model tended to bounce off of the ground during footstrike, rather than remain anchored. The first larger peak of ground force is the result of the foot landing first on the forefoot, then bringing down the heel (at which point the force reaches a maximum). Then, however, the foot begins to bounce off of its heel, upward. At this point, the forefoot again makes strong contact with the ground, providing leverage for the foot to push off (as reflected in the second peak of ground force). This rocking back and forth of the foot, or bouncing from forefoot to heel and back, was a consistent behavior observed in simulations of the Shoe Model.

The plots of ankle force over time are somewhat consistent with those of the Basic Model and Shoe Model, but with important differences. The first of these is the erratic changes in force after about 0.017 seconds. These results are caused by the oscillatory motion of the points that make up the shoe during liftoff. These motions are present even at very small time steps, suggesting that our method of assessing and applying damping may be insufficient in this formulation of the model. More generally, ankle force appears to generally correlate with the ground force, consistent with the other models.

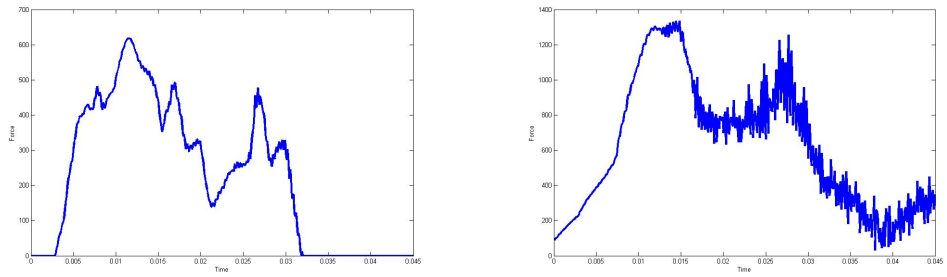

(a) Ground Force (b) Ankle Force

Figure 14: Results for a typical set of parameters using the Shoe Model (forefoot strike). Parameters for these results are given in Table 6. We use a time-step of 0.000002 seconds, sampling data every .0001 seconds.

4.3.2 Varying Shoe Shapes

We considered the effect upon footstrike of modifying the shape of the shoe. By keeping all other parameters equal and running simulations for each of three different shoe shapes (large heel, neutral, and large forefoot, shown in Figure 15), we were able to collect and compare data on ground forces in each case. These are presented in Figure 16. The ground impact forces

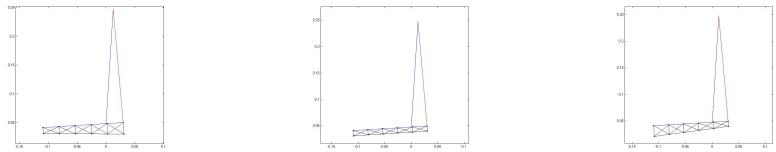

(a) Large Heel (b) Neutral (c) Large Forefoot

Figure 15: Three different shoe shapes.

in these cases were quite different. The large heel case produced the largest maximum force but also produced a smoother force plot than the neutral case. However, it is important to note that, in the simulation, the shoe with a large heel did not quite take off completely; the forefoot came back down and brushed the ground after takeoff, resulting in the small spike of force occurring at about 0.032 seconds.

The shoe with the large forefoot, on the other hand, produced the lowest peak impact forces and the smoothest overall plot of ground force over time.

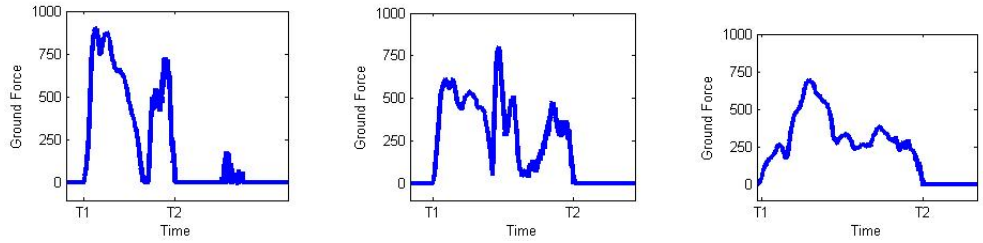

(a) Large Heel (b) Neutral (c) Large Forefoot

Figure 16: Ground force versus time plots for the three different shoe shapes shown in Figure 15. Forces are in Newtons and time is in seconds. $T1$ denotes touchdown and $T2$ denotes takeoff.

The peak impact forces were approximately 900 Newtons for the large-heel shoe, 800 Newtons for the neutral shoe, and 700 Newtons for the large-forefoot shoe. This result is perhaps surprising, since most running shoes are designed with thicker heels than forefeet. However, these results also deal only with forefoot strike.

5 Conclusion and Future Work

The models presented here address several key questions relating to footstrike in running. Results from the Basic Model suggest that impact forces are higher in heelstriking than in forefoot striking and that forefoot striking is more efficient and effective. Our search for optimal parameters also gives an indication of the most effective physical parameters for footstrike; these include a ratio of heel length to foot length that is similar to the actual value.

Results from the Body Model demonstrate an accurate reproduction of an important result in footstrike biomechanics, the force-time plot of ground impact force. They also suggest that forces in the ankle during footstrike may be much higher than those experienced by the foot on impact, and that knee forces may be somewhat higher than impact forces. Using our model of the ground, we also obtained results on how ground properties affect the total impulse imparted to the foot.

Using the Shoe Model, we obtained results suggesting that a shoe with a thicker forefoot may allow for less ground impact during a forefoot strike, as compared to a neutral shoe and one with a thicker heel. However, during

simulations, the shoe exhibited oscillatory motion of its points, suggesting the need for better parameters or an improved model of shoe behavior.

These results, while not definitive, may provide a foundation for future research and indicate possible lines of inquiry. In particular, we hope to have shown that there are exciting possibilities for further research into models and simulations that can accurately replicate experimental results such as the force-time plot as well as make predictive statements about the efficiency or optimality of hypothetical foot and shoe parameters.

The models presented here may provide a basis for further exploration. There are several promising ways in which this research can be extended in the future.

One way to make the models more realistic is to implement additional structures of the foot. These include, most significantly, the arch and the toes. Another is to combine the Body Model and Shoe Model in order to produce a more realistic and detailed simulation. Finally, three-dimensional dynamics could be incorporated.

Another modeling change we have considered, but not yet used to collect results, is incorporating time-dependent spring constants for the muscles. Changing spring properties have been shown to better model force-time plots in certain cases [13].

In any of these directions, there is much work to be done. With continued research in these directions, it is hoped that research can continue to shed light on the subject of footstrike and biomechanics.

6 Appendix

Parameter	Typical Value	Description
$\left\vert\vec{l}_f\right\vert$	0.14	length of foot
$\left\vert\vec{l}_s\right\vert$	0.20	length of shank
ρ_f	1	density of foot
ρ_s	1	density of shank
α_h	0.20	ratio of heel length to foot length
α_a	0.25	ratio of ankle length to shank length
θ_{rest}	0.6π	resting angle between foot and shank
ω_s	19	angular velocity of shank
μ_t	-3	spring property of tibialis
α_t	3	spring property of tibialis
μ_c	-4.6	spring property of calf
α_c	4.3	spring property of calf
$\frac{d\vec{r}_{s1}}{dt}$	$\begin{bmatrix} 0.5 \\ -2.7 \end{bmatrix}$	initial velocity of $\vec{r}_{s1}$
$\frac{d\theta_f}{dt}$	-26	initial angular velocity of foot
$cols$	60	number of columns of points in ground model
$rows$	4	number of rows of points
m_{pt}	0.001	mass of each point in ground model
k_{pt}	1300	spring constant of each spring in ground model
b_{pt}	0.7	damping coefficient for each spring
θ_{f0}	1.05π	initial angle of foot (forefoot strike)
θ_{s0}	0.5π	initial angle of shank (forefoot strike)
θ_{f0}	0.95π	initial angle of foot (heel strike)
θ_{s0}	0.4π	initial angle of shank (heel strike)

Table 4: Parameters of the lower leg for a typical simulation of the Basic Model.

Parameter	Typical Value	Description
$\left\vert\vec{l_f}\right\vert$	0.14	length of foot
$\left\vert\vec{l_s}\right\vert$	0.20	length of shank
$\left\vert\vec{l_b}\right\vert$	0.10	length of femur
ρ_f	1	density of foot
ρ_s	1	density of shank
ρ_q	1	density of femur
m_b	6	mass of body
α_h	0.20	ratio of heel length to foot length
α_a	0.25	ratio of ankle length to shank length
θ_{rest}	0.59π	resting angle between foot and shank
μ_t	-3	spring property of tibialis
α_t	3	spring property of tibialis
μ_c	-4.6	spring property of calf
α_c	4.3	spring property of calf
k_q	200000	spring constant of thigh muscle group
$\frac{d\vec{r}_{s1}}{dt}$	$\begin{bmatrix} 0 \\ -2 \end{bmatrix}$	initial velocity of $\vec{r}_{s1}$
$\frac{d\vec{r}_b}{dt}$	$\begin{bmatrix} -5 \\ -2 \end{bmatrix}$	initial velocity of body
$\frac{d\theta_f}{dt}$	-26	initial angular velocity of foot

Table 5: Parameters of the Body Model for a typical simulation.

Parameter	Typical Value	Description
$\left\vert\vec{l}_f\right\vert$	0.14	length of foot
$\left\vert\vec{l}_s\right\vert$	0.20	length of shank
ρ_f	2	density of foot
ρ_s	6	density of shank
α_h	0.20	ratio of heel length to foot length
α_a	0.25	ratio of ankle length to shank length
θ_{rest}	0.58π	resting angle between foot and shank
ω_s	19	angular velocity of shank
μ_t	-3	spring property of tibialis
α_t	3	spring property of tibialis
μ_c	-5.0	spring property of calf
α_c	5.5	spring property of calf
$\frac{d\vec{r}_{s1}}{dt}$	$\begin{bmatrix} 0.5 \\ -2.7 \end{bmatrix}$	initial velocity of $\vec{r}_{s1}$
$\frac{d\theta_f}{dt}$	-19	initial angular velocity of foot
$cols$	10	number of columns of points in the ground
$rows$	3	number of rows of points in the ground
m_{pt}	0.02	mass of each point in the ground
k_{pt}	50000	spring constant of each spring in the ground
b_{pt}	100	damping coefficient for each point in the ground
$cols$	6	number of columns of points in the shoe
$rows$	2	number of rows of points in the shoe
m_{pt}	0.001	mass of each point in the shoe
k_{pt}	100000	spring constant of each spring in the shoe
b_{pt}	1	damping coefficient for each point in the shoe
θ_{f0}	1.04π	initial angle of foot
θ_{s0}	0.48π	initial angle of shank

Table 6: Parameters of the Shoe Model for a typical simulation.

References

[1] D. E. Lieberman, et al., Foot strike patterns and collision forces in habitually barefoot versus shod runners, Nature 463.28 (2010) 531–4.

[2] T. A. McMahon, Muscles, Reflexes, and Locomotion, Princeton University Press, 1984.

[3] D. Lieberman, et al., Biomechanics of foot strikes, http://www.barefootrunning.fas.harvard.edu/4BiomechanicsofFootStrike.html.

[4] M. Cluss, et al., The indirect measurement of biomechanical forces in the moving human body, American Journal of Physics 74.2 (2006) 102–8.

[5] S. Jacob, et al., Three-dimensional foot modeling and analysis of stresses in normal and early stage hansen's disease with muscle paralysis, Journal of Rehabilitation Research and Development 36.3.

[6] K. G. M. Gerritsen, et al., Direct dynamics simulation of the impact phase in heel-toe running, Journal of Biomechanics 28.6 (1995) 661–8.

[7] M. Zhang, et al., Computationally modeling the foot-insole interface, Studies in Computational Intelligence 55 (2007) 311–21.

[8] S. J. P. Ahmet Erdemir, Changes in foot loading following plantar fasciotomy: A computer modeling approach, Journal of Biomechanical Engineering 126.2 (2004) 237–43.

[9] D. A. W. Stephen H. Scott, Biomechanical model of the human foot: Kinematics and kinetics during the stance phase of walking, Journal of Biomechanics 26.9 (1993) 1091–104.

[10] A. Inc, Ankle anatomy, http://www.nlm.nih.gov/medlineplus/ency/imagepages/19840.htm.

[11] H. Gray, Anatomy of the human body, www.bartleby.com/107/.

[12] C. R. Huock, et al., A genetic algorithm for function optimization: A matlab implementation, http://citeseerx.ist.psu.edu/viewdoc/download?doi=10.1.1.22.4413.

[13] I. Hunter, A new approach to modeling vertical stiffness in heel-toe distance runners, Journal of Sports Science and Medicine 2 (2003) 139–43.